
Towards Open-set Camera 3D Object Detection

Zhuolin He¹, Xinrun Li², Heng Gao¹, Jiachen Tang¹, Shoumeng Qiu¹,
Wenfu Wang², Lvjian Lu², Xuchong Qiu², Xiangyang Xue¹, Jian Pu¹

¹Fudan University

²Bosch Corporate Research

<https://github.com/NickHezhuolin/OS-Det3D>

Abstract

Traditional camera 3D object detectors are typically trained to recognize a predefined set of known object classes. In real-world scenarios, these detectors may encounter unknown objects outside the training categories and fail to identify them correctly. To address this gap, we present OS-Det3D (Open-set Camera 3D Object Detection), a two-stage training framework enhancing the ability of camera 3D detectors to identify both known and unknown objects. The framework involves our proposed 3D Object Discovery Network (ODN3D), which is specifically trained using geometric cues such as the location and scale of 3D boxes to discover general 3D objects. ODN3D is trained in a class-agnostic manner, and the provided 3D object region proposals inherently come with data noise. To boost accuracy in identifying unknown objects, we introduce a Joint Objectness Selection (JOS) module. JOS selects the pseudo ground truth for unknown objects from the 3D object region proposals of ODN3D by combining the ODN3D objectness and camera feature attention objectness. Experiments on the nuScenes and KITTI datasets demonstrate the effectiveness of our framework in enabling camera 3D detectors to successfully identify unknown objects while also improving their performance on known objects.

1 Introduction

Detecting 3D objects from image data is a core challenge in autonomous vehicles [23, 22, 40]. Traditional camera 3D object detectors are typically trained to recognize a predefined set of *known object* classes (e.g., cars, pedestrians, bicycles) under closed-set conditions. However, in real-world scenarios, these detectors may encounter *unknown objects* (e.g., animals or trash bins on the road), posing significant safety risks and limiting their practical utility [3]. As a result, there has been growing interest in open-set 3D object detection, where 3D detectors should detect *known objects* and *unknown objects* at the same time [6].

Previous methods in 2D [29, 27, 35, 17, 12, 44] or researches on LiDAR [6, 7] for detecting unknown or novel objects typically rely on proposing object regions and assigning each a confidence score. To effectively detect unknown or novel 3D objects, this issue can be divided into two manageable sub-tasks: initially discovering general 3D objects and distinguishing the unknown 3D objects from these initial discoveries.

Recent works [21, 5] implement the 3DETR [28] as a class-agnostic 3D object detector to propose 3D object regions for discovering unknown or novel objects. However, it is observed that the class-agnostic 3D detector frequently overlooks unknown objects in autonomous scenarios. A key reason for this failure is its high dependence on labeled data supervision during training, which limits its capacity to generalize to unknown objects. Traditional object detectors are penalized for detecting unlabeled objects in the background during training, discouraging them from identifying unknown objects. Previous works [18, 16] design classification-free methods in 2D to avoid suppressing

unannotated objects in the background. However, no such research has been conducted in 3D. Directly applying such classification-free methods in 3D could potentially lead to a catastrophic decline in model detection performance, as shown in Tab. 5.

Another problem associated with the region proposal method is the class-agnostic nature of the network’s prediction results. It becomes challenging to identify unknown objects among them. Joseph *et al.* [17] propose an auto-labeling step that selects proposals with high objectness scores and minimal overlap with known ground-truth instances as pseudo-unknowns. However, this method may mistakenly classify unlabeled known objects as unknowns during training, which impairs the model’s detection performance by incorporating incorrect data.

Motivated by the aforementioned observations, we present a two-stage training framework, Open-set Camera 3D Object Detection (OS-Det3D), which enhances the ability of camera 3D detectors to recognize unknown 3D objects. Our framework consists of two main components: a 3D Object Discovery Network (ODN3D) and a Joint Objectness Selection (JOS). The ODN3D uses a Geometric-only Hungarian (GeoHungarian) match algorithm to sample class-agnostic instances and a 3D objectness score to help the model learn the geometric features of these instances, significantly enhancing its capability to detect novel 3D objects. The JOS generates object proposal regions from ODN3D’s objectness scores and estimates the bird’s-eye view (BEV) region feature attention value of the camera detector to distinguish potential unknown objects. We then train a closed-set camera 3D detector with these identified potential unknown objects. This approach enables the detector to recognize both known and unknown objects without modifying its architecture. To our knowledge, we are the first to introduce work on open-set camera 3D object detection.

To validate our framework, we divide the nuScenes dataset into two splits for experimentation. Results show that OS-Det3D improves detection performance for both known and unknown objects. Additionally, ODN3D outperforms state-of-the-art open-set 3D detection methods on the KITTI dataset, improving Recall by 24.4% and AP by 23.5% on unknown objects. Ablation studies and extensive analysis demonstrate the effectiveness of OS-Det3D.

2 Related Work

Closed-set 3D Object Detection. In closed-set 3D object detection, integrating LiDAR and camera sensors has led to significant advancements. Recent LiDAR-based studies [9, 43, 37] have shown high accuracy in detecting and localizing 3D objects within known categories, leveraging LiDAR’s precision in distance measurement. Concurrently, camera-based methods [22, 23] capture detailed texture and color information, enhancing object classification with rich visual data. Innovative fusion techniques [2, 24, 26] combine the strengths of both modalities, substantially improving detection accuracy. Despite these advancements, these methods are limited to recognizing known objects and struggle to identify unknown objects, posing a key challenge in open-set scenarios.

Class-agnostic Region Proposal Network. In the realm of 2D object proposal, early works [1, 11, 33, 46, 34] emphasized category-independent proposals, aiming to identify all objects in an image regardless of their category. Addressing the limitations of these methods, Kim *et al.* [18] proposed an object localization network (OLN), which focuses on class-agnostic objectness via learning centerness [32], thereby facilitating the detection of unannotated, novel objects. Extending this concept, Wang *et al.* [35] developed a pairwise affinity predictor within the traditional learning-free paradigm to discover unannotated objects, while GOOD [16], paralleling OLN, advanced the approach by integrating geometric cues for enhanced generalization of the detector. Our work develops ODN3D specifically designed to detect general 3D objects. By leveraging geometric cues and a class-agnostic approach, ODN3D achieves superior generalization for unknown categories.

Open-set And Open World Object Detection. The concept of the open-set object detection problem was first introduced by Dhamija *et al.* [10] and has been further explored by subsequent research [44, 41, 30, 12]. In this setting, the model is provided with labels for certain known category instances during training but is required to identify both known and unknown objects at the test time. Extending beyond open-set object detection, Joseph *et al.* [17] proposed a novel setting called Open World Object Detection. This setting aims to enable models to recognize objects of known categories while detecting and incrementally learning to identify previously unseen new categories. Further advancing Open World Object Detection, Gupta *et al.* [14] introduced the Open World Detection Transformer (OW-DETR), which uses a pseudo-labeling scheme to supervise unknown object detection. In this

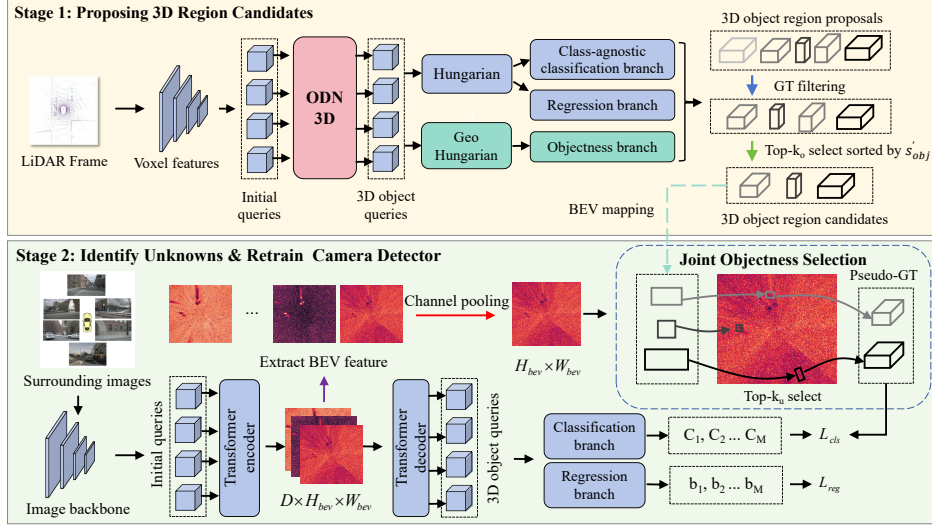


Figure 1: **Proposed OS-Det3D Training Framework.** ODN3D denotes the 3D Object Discovery Network. Both $\text{top-}k_o$ and $\text{top-}k_u$ are hyperparameters. In stage 1, voxel features from a LiDAR frame are extracted using the LiDAR backbone and input into ODN3D’s encoder-decoder along with a set of initial queries. At the decoder output, each 3D object query is processed by 3 different branches. Our objectness branch outputs the geometric confidence s'_{obj} of a query being an object. The output of ODN3D is a set of 3D object region proposals. In ground truth (GT) filtering, we filter 3D object region proposals that overlap with the instances of known categories. After GT filtering, the $\text{top-}k_o$ proposals are selected as 3D object region candidates. In Stage 2, we extract bird’s-eye view (BEV) features from the final layer of the camera encoder and perform a channel pooling step. JOS computes the BEV attention value in the BEV region of each 3D object region candidate to select the $\text{top-}k_u$ candidates as the pseudo-GT of unknown objects. Finally, these pseudo-GT of unknown objects are input to the classification branch of the camera detector.

scheme, unmatched object proposals with high backbone activation are selected as unknown objects. Shifting the focus to 3D object detection, Wong *et al.* [38] first introduced the open-set 3D Instance Segmentation network with LiDAR, uniquely designed for 3D space open-set conditions. Recent research such as MLUC [6] and REAL [7] has focused on addressing the detection or segmentation of unknown objects using LiDAR detectors. However, beyond these studies, exploration into camera-based open-set 3D detection remains significantly underdeveloped. Our research develops a novel framework to enable camera 3D detectors to identify unknown 3D objects effectively.

3 Open-set Camera 3D Object Detection

We formulate the open-set 3D object detection problem in Sec. 3.1. Fig. 1 shows the overall architecture of the proposed open-set camera 3D object detection framework, OS-Det3D. This framework enhances a closed-set camera 3D detector to achieve open-set detection capabilities through two key components: (i) a 3D Object Discovery Network (ODN3D) (described in Sec. 3.2) for generating 3D object region proposals; (ii) a Joint Objectness Selection (JOS) (detailed in Sec. 3.3) for selecting appropriate proposals as pseudo ground truth (pseudo-GT) of unknown objects. The entire framework is trained using a two-stage training process, as explained in Sec. 3.4.

3.1 Problem Formulation

Let $\mathcal{K} = \{1, 2, \dots, C_K\}$ represent the set of known object categories, where C_K is the number of known categories. Let $\mathcal{U} = \{C_K + 1, \dots, C_K + C_U\}$ denote the set of unknown classes, where C_U is the number of unknown categories. In an open-set condition, the training dataset $\mathcal{D}_{\text{train}}$ consists only of known categories \mathcal{K} , while the test dataset $\mathcal{D}_{\text{test}} = \mathcal{K} \cup \mathcal{U}$ includes both known and unknown categories. The test dataset classes are denoted as $\{1, 2, \dots, C_K, C_K + 1, C_K + 2, \dots, C_K + C_U\}$.

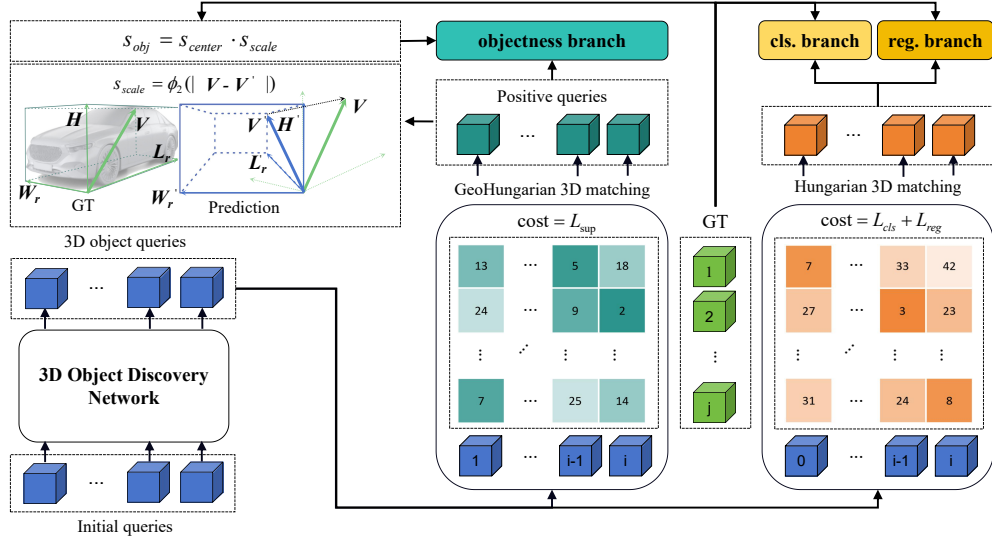


Figure 2: **Overview of ODN3D.** We retain the original Hungarian matching, classification branch, and regression branch of the transformer-based architecture in ODN3D. At the ODN3D’s decoder output, we designed a GenHungarian matching algorithm to sample 3D object queries. Hungarian matching calculates the cost matrix with cost values that are category-dependent, while GeoHungarian matching is category-independent and focuses solely on geometric cues, the positive queries sampled by these two matching strategies may differ. Based on the GenHungarian matching algorithm, we further introduced an objectness branch to form the objectness score s_{obj} , which assesses the geometric localization quality of these positive queries.

The training dataset $\mathcal{D}_{\text{train}} = \{\mathcal{I}, \mathcal{Y}\}$ contains images $\mathcal{I} = \{I_1, \dots, I_m\}$ with 3D annotations $\mathcal{Y}_{\text{train}} = \{\mathbf{b}_i \mid i = 1, 2, \dots, k\}$, where each annotation $\mathbf{b}_i = [c, x, y, z, w, l, h, r]$. In these annotations, c represents the known class in $\mathcal{D}_{\text{train}}$, (x, y, z) specifies the position of the center point of the 3D bounding box, (w, l, h) indicates the dimensions, and r denotes the rotation (yaw angle).

During the training and testing process, all categories in \mathcal{U} are collectively treated as a single category. Furthermore, instances from \mathcal{U} are not visible to the open-set 3D detector during training; the model is trained exclusively using instances from \mathcal{K} . A camera open-set 3D detector is trained to detect unknown objects from unknown categories \mathcal{U} while recognizing objects in known categories \mathcal{K} .

3.2 3D Object Discovery Network

ODN3D adopts a transformer-based network architecture similar to Object DGCNN [37]. As illustrated in Fig. 2, ODN3D incorporates a GeoHungarian matching algorithm that samples queries based on geometric cues. We also introduce a 3D objectness score rewarding the model to learn geometric features by measuring the geometric quality of those queries. These designs enhance ODN3D’s cross-category generalization ability. The details of the GeoHungarian matching algorithm and 3D objectness score are as follows.

GeoHungarian Matching. DETR3D [36] established a correspondence between the ground truth and the queries via Hungarian algorithm [20]. Building on this approach, we reformulate the geometry-only bipartite matching problem defined as follows:

$$\sigma' = \arg \min_{\sigma \in \mathcal{P}} \sum_{j=1}^M \mathcal{L}_{L1}(b_j, \hat{b}_{\sigma(j)}), \quad (1)$$

where \mathcal{P} denotes the set of permutations, M denotes the number of ground-truth boxes, b denotes the geometric annotation of $[x, y, z, w, l, h, r]$, $\sigma(\ast)$ returns the corresponding index of the ground-truth bounding box, and \mathcal{L}_{box} is the $L1$ loss for bounding box parameters. Our final set-to-set loss is also

reformulated as

$$\mathcal{L}_{sup} = \sum_{j=1}^M \mathcal{L}_{L1}(b_j, \hat{b}_{\sigma'(j)}). \quad (2)$$

This design leads the model to calculate one-to-one matches between queries and the ground truth solely based on 3D geometric information during training. Queries that closely match the ground truth in geometric terms are presented as positive examples in the matching results.

3D Objectness Score. First, a ground truth 3D bounding box $b_i = [c, x, y, z, w, l, h, r]$ can be divided into localization part (x, y, z) and scale part (w, l, h, r) , disregarding class c . The applies to a 3D object query \hat{b}_i is the same. Our intuition is that they represent different attributions of a bounding box. Thus, our 3D objectness score encompasses measurements of 3D localization and scale, as illustrated in Fig. 2 in the top-left corner.

For localization measurement, we calculate the $L1$ distance between the center point $O = [x, y, z]$ of ground truth 3D bounding box and the center point \hat{O} of 3D object query. For scale measurement, to address the inconsistency in units between r (measured in radians) and w, l, h (measured in meters) we reformulate the scale information as $\vec{L} = [l, 0, 0]^\top$, $\vec{W} = [0, w, 0]^\top$, and $\vec{H} = [0, 0, h]^\top$. The yaw angle r can be represented by the rotation matrix R_z . By applying $R_z(r)$ to \vec{L} and \vec{W} , we obtain the rotated vectors $\vec{L}_r = R_z(r) \cdot \vec{L}$ and $\vec{W}_r = R_z(r) \cdot \vec{W}$, effectively aligning them with the 3D object’s orientation. For the scale of ground truth 3D bounding box, we can describe it as a vector $\vec{V} = [\vec{L}_r, \vec{W}_r, \vec{H}]^\top$. And the prediction 3D bounding box is denoted as $\hat{\vec{V}}$, we use the $L1$ distance between vectors \vec{V} and $\hat{\vec{V}}$ as a measure of scale. The centeredness score and scale score of queries are calculated as $s_{center} = \phi_1(\|O - \hat{O}\|)$ and $s_{scale} = \phi_2(\|\vec{V} - \hat{\vec{V}}\|)$. Here ϕ_1 and ϕ_2 are two Gaussian kernel functions which can be written as $\exp(-\|\mathbf{x} - \hat{\mathbf{x}}\|^2 / 2\tau)$, wherein \mathbf{x} and $\hat{\mathbf{x}}$ are two distribution vectors, parameter τ is used to normalize centeredness score and scale score. The objectness score is $s_{obj} = \sqrt{s_{center} \cdot s_{scale}}$. With the ground truth objectness scores s_{obj} set to 1. The objectness loss of our objective branch in the form of $L1$ can be written as $\mathcal{L}_{obj} = \mathcal{L}_{L1}(s_{obj}, \hat{s}_{obj})$.

3.3 Joint Objectness Selection

Although ODN3D generates 3D object region proposals, distinguishing between known and unknown objects within these proposals remains challenging. To overcome this limitation, the JOS module is designed to refine the selection of potential unknown objects from the 3D object region proposals.

After filtering 3D object region proposals with ground truth, we assume that high objectness scores are more likely to correspond to actual objects, while low scores are more likely to indicate regions without objects. We sort 3D object region proposals by their objectness scores s'_{obj} and select the top- k_o of them as 3D object region candidates.

Next, we utilize the BEV feature activation from the camera 3D detector. The magnitude of the BEV feature activation indicates the presence of a known object at that BEV spatial position, enabling us to compute the confidence for a known object within a BEV 2D bounding box. This implies that 3D object candidates with high feature attention responses are more likely to be known category objects, while those with low feature attention responses are likely to be unknown objects or noise.

Building on OW-DETR [14], we compute the attention score s_{att} for each BEV region using its corresponding BEV feature. Specifically, these BEV regions are mapped from the 3D region candidates and only maintain the scale w and l . Considering the rotation (yaw angle) r in 3D space, s_{att} is defined as follows:

$$s_{att} = \frac{1}{w \times l} \sum_{i=1}^w \sum_{j=1}^l A(x + i \cdot \cos(r) - j \cdot \sin(r), y + i \cdot \cos(r) + j \cdot \sin(r)), \quad (3)$$

where $A \in \mathbb{R}^{w \times l}$ is the BEV feature map averaged over the number of channels D . Combining the two scores mentioned above, 3D object region candidates with high objectness scores and low feature attention scores are more aligned with our criteria for being selected as potential unknown objects.

To refine the distinction between known and unknown based on the aforementioned scores, we calculate the joint objectness score as $s_{jos} = s'_{obj} \cdot (1 - s_{att})$. We then re-rank these candidates

based on s_{jos} and select the top- k_u candidates as our pseudo-GT. The objectness score s'_{obj} serves as a weight ω of pseudo-GT, contributing to the loss computing of the classification branch.

3.4 Two-stage Training

First Stage. BEVFormer [23] is employed as our camera 3D object detector. BEVFormer and ODN3D are trained exclusively with instances of known classes. The loss formulation used in this stage is as follows:

$$\mathcal{L}_{camera} = \mathcal{L}_{cls}^{\mathcal{K}} + \mathcal{L}_{reg}, \quad \mathcal{L}_{LiDAR} = \mathcal{L}_{cls}^{\{0,1\}} + \mathcal{L}_{reg} + \mathcal{L}_{obj}, \quad (4)$$

where the loss terms for classification, bounding box regression and objectness scoring are denoted by \mathcal{L}_{cls} , \mathcal{L}_{reg} and \mathcal{L}_{obj} , respectively. The standard focal loss [25] is employed for formulating \mathcal{L}_{cls}^* . The term $\mathcal{L}_{cls}^{\mathcal{K}}$ refers to \mathcal{L}_{cls} when training to classify each known class \mathcal{K} , while $\mathcal{L}_{cls}^{(\mathcal{K})}$ signifies the binary classification loss \mathcal{L}_{cls} where known classes \mathcal{K} are grouped into a single category. \mathcal{L}_{reg} and \mathcal{L}_{obj} are formulated using the standard *L1* regression loss. ODN3D proposes a set of 3D object region proposals. Each proposal includes a predicted objectness score s'_{obj} . After ground truth filtering, we select top- k_o proposals as 3D objects region candidates, ranked by s'_{obj} .

Second Stage. We extract BEV features from the last layer of the BEVFormer encoder and process them through pooling operations as input for the JOS module. In the JOS module, the 3D object candidates are mapped into the BEV regions for further processing. The JOS would select top- k_u proposals as pseudo-GT $\mathcal{Y}_{pseudo-GT}$ after computing the features attention value of each BEV region. Along with the original training classification labels ($\mathcal{Y}_{train} = \mathcal{Y}_{GT}$), we form an updated training label set: $\mathcal{Y}_{train} = \mathcal{Y}_{pseudo-GT} \cup \mathcal{Y}_{GT}$. In this stage, we only train the camera 3D object detector using the following loss formulation:

$$\mathcal{L}_{camera} = \mathcal{L}_{cls}^{\mathcal{K}+1} + \mathcal{L}_{reg}, \quad \mathcal{L}_{cls}^{\mathcal{K}+1} = \mathcal{L}_{cls}^{\mathcal{K}} + \sum_{i=1}^{\text{top-}k_u} \omega_i \mathcal{L}_{cls}^{(\mathcal{U})}(c_i, \hat{c}_{\sigma(i)}). \quad (5)$$

Here, ω denotes the weight factor for the unknown object classification. The weight of the pseudo-labels is adjusted using objectness score s'_{obj} from ODN3D predictions. The term $\mathcal{L}_{cls}^{(\mathcal{U})}$ refers to unknown classes \mathcal{U} are grouped into a single category. During the inference, images are used as only input.

4 Experiments

4.1 Implementaion

Datasets. We evaluate our method on two datasets, KITTI [13] and nuScenes [4]. Same as MLUC [6], in KITTI, 3 common classes (*car*, *pedestrian*, *cyclist*) are classified as known objects, while the *van* and *truck* are used as the unknown classes. The nuScenes dataset features 23 object classes grouped into 11 major categories, which serve as the basis for our class division. In **nuScenes Split 1**, we classify 3 common classes (*car*, *pedestrian*, *bicycle*) as known, with the remaining classes treated as unknown. In **nuScenes Split 2**, we add *barriers* and *construction vehicles* to the known classes, while the remaining 6 classes (*truck*, *bus*, *trailer*, *motorcycle*, *traffic cone*, *debris*) are designated as unknown. Detail see the Sec. A appendix.

Evaluation metrics. As for the KITTI dataset, we adopt the evaluation metrics of MLUC [6]. Same in the nuScenes dataset, we utilize the mean Average Precision ($\text{mAP}_{\text{known}}$) to assess the performance of known objects, while reporting ($\text{Recall}_{\text{unk}}$) and unknown Average Precision (AP_{unk}) for the unknown objects. These metrics are evaluated based on the standard nuScenes benchmark [4].

Model details. We base ODN3D on Object OGCNN [37]. BEVFormer [23] is chosen as our camera 3D detector. Both models implement from mmdetection3d [8]. In stage 1, ODN3D is trained with the instances of *known categories* under closed-set conditions for 20 epochs. Under the same closed-set setting as ODN3D, we train BEVFormer for 18 epochs. In stage 2, we reload the pre-trained weights of the closed-set BEVFormer into our framework’s BEVFormer, excluding the weights of the classification branch. BEVFormer is trained to learn unknown objects for another 6 epochs. We discuss implementation details in Sec. B of the appendix.

Table 1: Open-set 3D object detection results on the nuScenes validation dataset. The dataset includes the following classes: car, pedestrian, bicycle, barriers, construction vehicles, truck, bus, trailer, motorcycle, traffic cone and debris. In **nuScenes Split 1**, car, pedestrian and bicycle are classified as known. In **nuScenes Split 2**, car, pedestrian, bicycle, barriers and construction vehicles are classified as known. The (Supervised) method includes the unknown classes in the training set and retrain the model, serving as the upper bound for open-set detection performance.

Methods	nuScenes Split 1			nuScenes Split 2		
	Recall _{unk} (↑)	AP _{unk} (↑)	mAP _{known} (↑)	Recall _{unk} (↑)	AP _{unk} (↑)	mAP _{known} (↑)
BEVFormer(Closed-set)	0	0	43.0	0	0	43.1
BEVFormer(Supervised)	52.5	20.5	44.6	52.3	42.6	43.1
DETR3D+OW-DETR[14]	12.7	0	38.9	0	0	31.8
BEVFormer+OW-DETR[14]	0.3	0	44.1	1.0	0	37.1
BEVFormer+RPN(naive)	16.7	0.7	44.3	25.9	1.4	42.5
BEVFormer+OS-Det3D(ours)	23.2	0.7	45.1	31.8	4.1	43.4

Table 2: Open-set 3D object detection results on KITTI validation set. Supervised method means we include the unknown classes in the training set, so it is the upper bound of the open-set detection performance. * present GT filtering. † present results from their papers.

Methods	Recall _{unk} (↑)	AP _{unk} (↑)	mAP _{known} (↑)
SECOND [39]	0	0	67.4
SECOND(Supervised)	94.3	76.4	72.6
MC-Dropout [27] †	-	2.6	64.1
OSIS [38] †	31.0	1.1	65.9
MLUC [6] †	50.0	9.7	66.8
ODN3D(ours)	74.4	3.0	74.5
ODN3D*(ours)	74.4	33.2	74.5

4.2 Open-set 3D Object Detection Results

To demonstrate the effectiveness of our method, we conduct detailed experiments on two different datasets nuScenes and KITTI. Furthermore, we divided the nuScenes dataset into two different data partitions: nuScenes Split 1, and nuScenes Split 2.

Results on nuScenes. Table 1 presents a comparison between two different pseudo-label generation approaches and our proposed OS-Det3D method. In BEVFormer(Closed-set), BEVFormer is trained only with known category labels, serving as a baseline for comparing known category detection performance with mAP_{known}. BEVFormer(Supervised) implies that BEVFormer is trained not only with known category labels but also includes ground truth from unknown categories. This is a reference upper bound for our model’s unknown detection performance with AR_{unk}, Recall_{unk} and AP_{unk}. The supervised model achieves an AP_{unk} of 20.5% under Split 1, only about 50% of that under nuScenes Split 2, which indicates that nuScenes Split 1 is more challenging than nuScenes Split 2 for the task of camera open-set 3D object detection.

Next, we adopt two different pseudo-label generation strategies on our basic model, detail see Sec. D. BEVFormer+OW-DETR refers to our adoption, same as OW-DETR [14] in this approach. DETR3D+OW-DETR extracts 2D plane features from 2D images, and BEVFormer+OW-DETR extracts the BEV features from the Transformer. We observed that methods relying on the camera’s intrinsic response struggle to obtain effective unknown labels for training. We adopt a naive RPN baseline based on [37] applying binary classification. Compared to this naive method, our proposed OS-Det3D improves a significant performance of detecting unknown on Recall_{unk} of 6.5% and AR_{unk} of 5.2% in nuScenes Split 1 setting. On the task of nuScenes Split 2, our improvement becomes even more significant.

Results on KITTI. Since the benchmark for open-set 3D object detection in KITTI only involves LiDAR 3D detectors, we present the results of ODN3D for a fair comparison. We follow the training and evaluation protocol of MLUC [6] and report the performance in Table 2. ODN3D evaluates all 3D

Table 3: Ablation of OS-Det3D Components on nuScenes Split 2 dataset.

ID	ODN3D	JOS	SW	Recall _{unk} (↑)	mAP _{known} (↑)
1	-	-	-	0	43.1
2	✓	-	-	21.8	35.2
3	✓	✓	-	31.7	42.5
4	✓	-	✓	26.9	41.2
5	✓	✓	✓	31.8	43.8

Table 4: Sensitivity Analysis of k_u on nuScenes Split 2 dataset.

k_u	mAP _{known} (↑)	AP _{unk} (↑)	Recall _{unk} (↑)
3	43.1	1.1	24.3
5	43.6	2.4	29.8
10	43.4	4.2	31.8
20	43.1	3.5	30.9
30	42.0	3.3	30.2

Table 5: Ablation of ODN3D on nuScenes Split 2 dataset.

ID	H	GH	OBJ	Recall _{unk} (↑)	AP (↑)
1	✓	-	-	50.1	62.2
2	-	✓	✓	50.9	4.2
3	✓	-	✓	49.8	58.7
4	✓	✓	✓	56.4	58.6

Table 6: Compares of different 3D objectness score on nuScenes Split 2 dataset.

ID	Methods	Recall _{unk} (↑)	AP (↑)
1	IOU3D[31]	48.2	52.0
2	RIOU3D[42]	50.0	52.0
3	OLN (3D-format) [18]	50.8	47.0
4	Ours	56.4	58.6

region proposal predictions as unknown objects, while ODN3D* evaluates the results after filtering out known categories. The results show that the ODN3D method achieves improved Recall_{unk} over all baselines, indicating our model’s superior ability to discover unknown instances. Furthermore, after ground truth filtering, ODN3D* outperforms MLUC [6] on AP_{unk} by 23.5%, demonstrating the effectiveness of our framework in utilizing ODN3D for pseudo-labeling tasks.

4.3 Ablation Study

Ablation of the OS-Det3D Components. We conduct ablation experiments on OS-Det3D to evaluate the impact of different components on nuScenes Split 2, as shown in Tab. 3. The standard BEVFormer model serves as the baseline, demonstrating basic detection performance for known classes. Initially, we incorporate only ODN3D predictions as pseudo-labels for unknown objects into the training. This enhances open-set detection but reduces the known class detection performance by 7.9% mAP_{known}. Next, we introduce the JOS module to better identify unknown instances from ODN3D proposals, improving Recall_{unk} by 10.1% and mAP_{known} by 7.3%. We also evaluate the impact of soft weighting (SW). Results indicate that SW enhances the model’s performance for both known and unknown categories. By comparison of rows 3,4,5, we found using JOS and SW individually both improve performance. However, adding SW on top of JOS does not provide the expected additional improvement, indicating that they have functional similarity in sample denoising. Finally, the best results are achieved by combining all components.

Ablation of the ODN3D Components. To study the contribution of each component in ODN3D, Table 5 presents the ablation study results on nuScenes Split 2. Object DGCNN trained with binary classification serves as our baseline. H, GH, and OBJ refer to Hungarian 3D matching, GeoHungarian matching and 3D objectness scores. AP represents Average Precision. We replace Hungarian matching with GeoHungarian matching in the baseline and update the model by calculating the objectness and regression loss for the GeoHungarian matching results, omitting the classification loss. The results show that removing Hungarian matching significantly degrades the model’s detection performance. we also experiment with the network using Hungarian matching and updating by calculating the objectness loss, which results in a 3.5% decrease in AP across all classes. Finally, we added an objectness branch to the baseline, employing GeoHungarian matching and calculating only the objectness loss for the matching results. This approach achieved the highest Recall_{unk}.

Sensitivity analysis on hyperparameters of JOS. As shown in Table 4, we analyze the model’s detection performance under different hyperparameter k_u settings for nuScenes Split 2, while keeping $k_o = 30$. We find out that a larger value of k_u hurts performance on mAP_{known}. When k_u is too small will result in a lack of sufficient unknown samples for the model to learn during training. Therefore, through validation, we set k_u to 10, which is a choice that balances the performance between known and unknown categories.

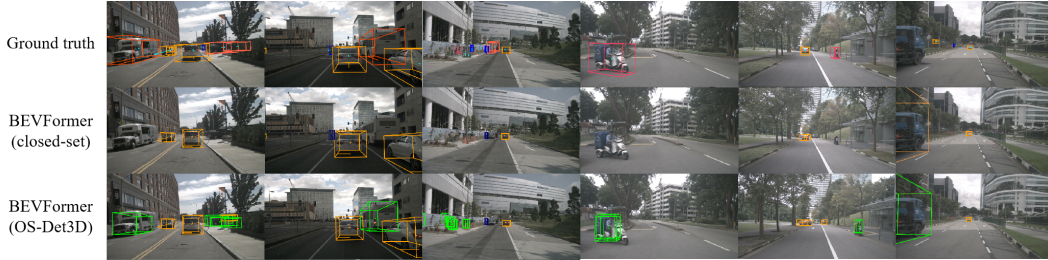


Figure 3: **Visualization Results on nuScenes Split 2.** The qualitative results showcase different outcomes. Row 1 corresponds to the ground truth (GT) with all classes: **car**, **pedestrian**, bicycle, barrier, construction vehicle, **truck**, **bus**, trailer, **motorcycle**, traffic cone, **debris** (trash bins, etc.). Row 2 to BEVFormer(Closed-set) which only focuses on detecting known classes (car, pedestrian, bicycle, barrier, construction vehicle) and row 3 to BEVFormer(OS-Det3D) which is able to identify **unknown** instances (truck, bus, trailer, motorcycle, traffic cone, debris). (Zoom in for a better view.)

Compares of different 3D objectness score. In this section, Tab. 6 compares different objectness scores on nuScenes Split 2. The baseline model used in the comparative experiments is complete ODN3D. In addition to IOU3D [31] and RIOU3D [42] commonly used in 3D object detection, we further adopt the OLN objectness score for 3D contexts by computing the geometric mean score of centeredness and IOU3D. Through comparison, we find that incorporating centeredness and constructing a more flexible scale description can both improve the detection capability of unknown objects to some extent in terms of Recall_{unk} . Therefore, by reasonably incorporating rotation angle information and effectively separating centeredness and scale to calculate the objectness score, we achieved the best performance in discovering unknown objects.

4.4 Qualitative Results

In Fig. 3, we provide qualitative results of known and unknown object detection. The first row represents the nuScenes ground truth with annotations for all categories, including debris items such as trash bins, as shown in column 3. The second row depicts BEVFormer trained on nuScenes Split 2 under closed-set conditions, serving as a comparison to our method’s results shown in the third row. It is evident that under closed-set conditions, BEVFormer can only detect known categories and fails to identify objects from untrained categories, such as buses, trucks and motorcycles. Conversely, with the aid of our training framework, BEVFormer gains the capability to detect unknown objects.

5 Conclusions

In this work, we introduce OS-Det3D framework to tackle the challenge of open-set 3D object detection with cameras in autonomous driving scenarios. By integrating ODN3D to discover 3D objects and JOS to select unknowns, OS-Det3D enhances the camera 3D detector’s ability to identify unknown 3D objects while improving performance on known categories. Experiments demonstrate its strong ability to detect both known and unknown objects. Despite these advancements, several limitations need to be addressed: (i) The framework’s ability to accurately identify unknown objects is not yet robust enough for real-world scenarios. (ii) Although the inference stage uses a camera-only pipeline, the training process still requires LiDAR data, which limits its practical application.

6 Broader Impact

In the real world, there are countless object categories, and labeling them all is impractical and costly. Most deep learning models for object detection are limited to a fixed set of known categories and struggle to generalize to novel or rare classes. This limitation restricts their usefulness in scenarios where unknown objects may appear. Our work introduces a novel method for open-set 3D object detection, enabling the discovery and detection of new classes without labeled data supervision. We believe this research will inspire further studies and advancements in creating more general and robust object detection models.

References

- [1] Alexe, B., Deselaers, T., Ferrari, V.: Measuring the objectness of image windows. *IEEE transactions on pattern analysis and machine intelligence* **34**(11), 2189–2202 (2012)
- [2] Bai, X., Hu, Z., Zhu, X., Huang, Q., Chen, Y., Fu, H., Tai, C.L.: TransFusion: Robust Lidar-Camera Fusion for 3d Object Detection with Transformers. *CVPR* (2022)
- [3] Bozhinoski, D., Di Ruscio, D., Malavolta, I., Pelliccione, P., Crnkovic, I.: Safety for mobile robotic systems: A systematic mapping study from a software engineering perspective. *Journal of Systems and Software* **151**, 150–179 (2019)
- [4] Caesar, H., Bankiti, V., Lang, A.H., Vora, S., Liong, V.E., Xu, Q., Krishnan, A., Pan, Y., Baldan, G., Beijbom, O.: nuscenes: A multimodal dataset for autonomous driving. *arXiv preprint arXiv:1903.11027* (2019)
- [5] Cao, Y., Yihan, Z., Xu, H., Xu, D.: Coda: Collaborative novel box discovery and cross-modal alignment for open-vocabulary 3d object detection. *Advances in Neural Information Processing Systems* **36** (2024)
- [6] Cen, J., Yun, P., Cai, J., Wang, M.Y., Liu, M.: Open-set 3d object detection. In: *2021 International Conference on 3D Vision (3DV)*. pp. 869–878. *IEEE* (2021)
- [7] Cen, J., Yun, P., Zhang, S., Cai, J., Luan, D., Tang, M., Liu, M., Yu Wang, M.: Open-world semantic segmentation for lidar point clouds. In: *Avidan, S., Brostow, G., Cissé, M., Farinella, G.M., Hassner, T. (eds.) Computer Vision – ECCV 2022*. pp. 318–334. *Springer Nature Switzerland, Cham* (2022)
- [8] Contributors, M.: MMDetection3D: OpenMMLab next-generation platform for general 3D object detection. <https://github.com/open-mmlab/mmdetection3d> (2020)
- [9] Deng, J., Shi, S., Li, P., Zhou, W., Zhang, Y., Li, H.: Voxel r-cnn: Towards high performance voxel-based 3d object detection. In: *Proceedings of the AAAI Conference on Artificial Intelligence*. vol. 35, pp. 1201–1209 (2021)
- [10] Dhamija, A., Gunther, M., Ventura, J., Boulton, T.: The overlooked elephant of object detection: Open set. In: *Proceedings of the IEEE/CVF Winter Conference on Applications of Computer Vision*. pp. 1021–1030 (2020)
- [11] Endres, I., Hoiem, D.: Category-independent object proposals with diverse ranking. *IEEE transactions on pattern analysis and machine intelligence* **36**(2), 222–234 (2013)
- [12] Fomenko, V., Elezi, I., Ramanan, D., Leal-Taixé, L., Osep, A.: Learning to discover and detect objects. *Advances in Neural Information Processing Systems* **35**, 8746–8759 (2022)
- [13] Geiger, A., Lenz, P., Urtasun, R.: Are we ready for autonomous driving? the kitti vision benchmark suite. In: *2012 IEEE conference on computer vision and pattern recognition*. pp. 3354–3361. *IEEE* (2012)
- [14] Gupta, A., Narayan, S., Joseph, K., Khan, S., Khan, F.S., Shah, M.: Ow-detr: Open-world detection transformer. In: *Proceedings of the IEEE/CVF Conference on Computer Vision and Pattern Recognition*. pp. 9235–9244 (2022)
- [15] He, K., Zhang, X., Ren, S., Sun, J.: Deep residual learning for image recognition. In: *Proceedings of the IEEE conference on computer vision and pattern recognition*. pp. 770–778 (2016)
- [16] Huang, H., Geiger, A., Zhang, D.: Good: Exploring geometric cues for detecting objects in an open world. *CoRR* **abs/2212.11720** (2022), <https://doi.org/10.48550/arXiv.2212.11720>
- [17] Joseph, K., Khan, S., Khan, F.S., Balasubramanian, V.N.: Towards open world object detection. In: *Proceedings of the IEEE/CVF conference on computer vision and pattern recognition*. pp. 5830–5840 (2021)

- [18] Kim, D., Lin, T.Y., Angelova, A., Kweon, I.S., Kuo, W.: Learning open-world object proposals without learning to classify. *IEEE Robotics and Automation Letters* **7**(2), 5453–5460 (2022)
- [19] Kingma, D.P., Ba, J.: Adam: A method for stochastic optimization. arXiv preprint arXiv:1412.6980 (2014)
- [20] Kuhn, H.W.: The hungarian method for the assignment problem. *Naval research logistics quarterly* **2**(1-2), 83–97 (1955)
- [21] Li, G., Li, X., Wang, Y., Zhang, S., Wu, Y., Liang, D.: Pseco: Pseudo labeling and consistency training for semi-supervised object detection. arXiv preprint arXiv:2203.16317 (2022)
- [22] Li, Y., Ge, Z., Yu, G., Yang, J., Wang, Z., Shi, Y., Sun, J., Li, Z.: Bevdepth: Acquisition of reliable depth for multi-view 3d object detection. In: *Proceedings of the AAAI Conference on Artificial Intelligence*. vol. 37, pp. 1477–1485 (2023)
- [23] Li, Z., Wang, W., Li, H., Xie, E., Sima, C., Lu, T., Qiao, Y., Dai, J.: Bevformer: Learning bird’s-eye-view representation from multi-camera images via spatiotemporal transformers. In: *European conference on computer vision*. pp. 1–18. Springer (2022)
- [24] Liang, T., Xie, H., Yu, K., Xia, Z., Lin, Z., Wang, Y., Tang, T., Wang, B., Tang, Z.: Bevfusion: A simple and robust lidar-camera fusion framework. *Advances in Neural Information Processing Systems* **35**, 10421–10434 (2022)
- [25] Lin, T.Y., Goyal, P., Girshick, R., He, K., Dollár, P.: Focal loss for dense object detection. In: *Proceedings of the IEEE international conference on computer vision*. pp. 2980–2988 (2017)
- [26] Liu, Z., Tang, H., Amini, A., Yang, X., Mao, H., Rus, D.L., Han, S.: Bevfusion: Multi-task multi-sensor fusion with unified bird’s-eye view representation. In: *2023 IEEE international conference on robotics and automation (ICRA)*. pp. 2774–2781. IEEE (2023)
- [27] Miller, D., Nicholson, L., Dayoub, F., Sünderhauf, N.: Dropout sampling for robust object detection in open-set conditions. In: *2018 IEEE International Conference on Robotics and Automation (ICRA)*. pp. 3243–3249. IEEE (2018)
- [28] Misra, I., Girdhar, R., Joulin, A.: An end-to-end transformer model for 3d object detection. In: *Proceedings of the IEEE/CVF International Conference on Computer Vision*. pp. 2906–2917 (2021)
- [29] Pham, T., Do, T.T., Carneiro, G., Reid, I., et al.: Bayesian semantic instance segmentation in open set world. In: *Proceedings of the European Conference on Computer Vision (ECCV)*. pp. 3–18 (2018)
- [30] Sarkar, H., Chudasama, V., Onoe, N., Wasnik, P., Balasubramanian, V.N.: Open-set object detection by aligning known class representations. In: *Proceedings of the IEEE/CVF Winter Conference on Applications of Computer Vision*. pp. 219–228 (2024)
- [31] Shi, S., Wang, X., Li, H.: Pointcnn: 3d object proposal generation and detection from point cloud. In: *Proceedings of the IEEE/CVF conference on computer vision and pattern recognition*. pp. 770–779 (2019)
- [32] Tian, Z., Shen, C., Chen, H., He, T.: Fcos: Fully convolutional one-stage object detection. In: *Proceedings of the IEEE/CVF international conference on computer vision*. pp. 9627–9636 (2019)
- [33] Uijlings, J.R., Van De Sande, K.E., Gevers, T., Smeulders, A.W.: Selective search for object recognition. *International journal of computer vision* **104**, 154–171 (2013)
- [34] Wang, J., Chen, K., Yang, S., Loy, C.C., Lin, D.: Region proposal by guided anchoring. In: *Proceedings of the IEEE/CVF conference on computer vision and pattern recognition*. pp. 2965–2974 (2019)
- [35] Wang, W., Feiszli, M., Wang, H., Malik, J., Tran, D.: Open-world instance segmentation: Exploiting pseudo ground truth from learned pairwise affinity. In: *Proceedings of the IEEE/CVF Conference on Computer Vision and Pattern Recognition*. pp. 4422–4432 (2022)

- [36] Wang, Y., Guizilini, V.C., Zhang, T., Wang, Y., Zhao, H., Solomon, J.: Detr3d: 3d object detection from multi-view images via 3d-to-2d queries. In: Conference on Robot Learning. pp. 180–191. PMLR (2022)
- [37] Wang, Y., Solomon, J.M.: Object dgcnn: 3d object detection using dynamic graphs. In: 2021 Conference on Neural Information Processing Systems (NeurIPS) (2021)
- [38] Wong, K., Wang, S., Ren, M., Liang, M., Urtasun, R.: Identifying unknown instances for autonomous driving. In: Conference on Robot Learning. pp. 384–393. PMLR (2020)
- [39] Yan, Y., Mao, Y., Li, B.: Second: Sparsely embedded convolutional detection. *Sensors* (2018)
- [40] Zhang, Y., Lu, J., Zhou, J.: Objects are different: Flexible monocular 3d object detection. In: Proceedings of the IEEE/CVF Conference on Computer Vision and Pattern Recognition (CVPR). pp. 3289–3298 (June 2021)
- [41] Zheng, J., Li, W., Hong, J., Petersson, L., Barnes, N.: Towards open-set object detection and discovery. In: Proceedings of the IEEE/CVF Conference on Computer Vision and Pattern Recognition. pp. 3961–3970 (2022)
- [42] Zheng, Y., Zhang, D., Xie, S., Lu, J., Zhou, J.: Rotation-robust intersection over union for 3d object detection. In: European Conference on Computer Vision. pp. 464–480. Springer (2020)
- [43] Zhou, Y., Tuzel, O.: Voxelnet: End-to-end learning for point cloud based 3d object detection. In: Proceedings of the IEEE conference on computer vision and pattern recognition. pp. 4490–4499 (2018)
- [44] Zhou, Z., Yang, Y., Wang, Y., Xiong, R.: Open-set object detection using classification-free object proposal and instance-level contrastive learning. *IEEE Robotics and Automation Letters* **8**(3), 1691–1698 (2023). <https://doi.org/10.1109/LRA.2023.3242169>
- [45] Zhu, B., Jiang, Z., Zhou, X., Li, Z., Yu, G.: Class-balanced grouping and sampling for point cloud 3d object detection. *arXiv preprint arXiv:1908.09492* (2019)
- [46] Zitnick, C.L., Dollár, P.: Edge boxes: Locating object proposals from edges. In: Computer Vision–ECCV 2014: 13th European Conference, Zurich, Switzerland, September 6–12, 2014, Proceedings, Part V 13. pp. 391–405. Springer (2014)

In this supplementary, we provide dataset splits (Sec. A), implementation details (Sec. B), details on Joint Objectness Selection (JOS) (Sec. C), details on OW-DETR baselines (Sec. D), sensitivity analysis of hyper-parameter k_o after Ground Truth filtering (Sec. E).

A Dataset Splits

Table 7: Dataset splits composition in the our evaluation. The semantics and the number of frames and instances (objects) across splits of two datasets are shown.

Dataset	KITTI Split		nuScenes Split 1		nuScenes Split 2	
	Known	Unknown	Known	Unknown	Known	Unknown
Semantic split	Car, Bicycle, Pedestrian	Van, Truck	Car, Bicycle, Pedestrian	Barrier, Bus, Debris Construction vehicle, Truck, Traffic cone, Trailer, Motorcycle	Car, Bicycle, Construction vehicle, Pedestrian, Barrier,	Bus, Truck, Trailer, Traffic cone, Motorcycle, Debris
Training scenes	-	-	700	-	700	-
Training frames	7481	-	28130	-	28130	-
Training instances	8690	-	608643	-	745731	-
Test scenes	-	-	150	-	150	-
Test frames	3769	-	6019	-	6019	-
Test instances	4845	1255	116732	70796	146102	41426

We evaluate our method on two datasets, KITTI [13] and nuScenes [4].

Same as MLUC [6] in KITTI, 3 common classes, *car*, *pedestrian* and *cyclist* are classified as known objects, while the *van* and *truck* are used as the unknown classes and not included during training in KITTI dataset.

The nuScenes dataset features 23 object classes grouped into 11 major categories. These 10 major categories serve as the foundation for our class division. The first split (**nuScenes Split 1**) focuses on 3 common classes (*car*, *pedestrian* and *bicycle*) as known, leaving 8 classes (*barrier*, *bus*, *construction vehicle*, *truck*, *traffic cone*, *trailer*, *motorcycle*, *debris*) as unknown. For the second split (**nuScenes Split 2**), we classify 5 classes (*car*, *pedestrian*, *bicycle*, *construction vehicle*, *barrier*) as known, with (*bus*, *truck*, *traffic cone*, *trailer*, *motorcycle*, *debris*) designated as unknown.

We designed the **nuScenes Split 2** dataset setup not only to validate the robustness of our method under different configurations in the nuScenes dataset. We also reference the **KITTI splits**, which involves including unknown categories that are geometrically similar to the known categories in the unknown split, while maintaining a similar ratio of known to unknown objects in the **nuScenes Split 2** validation dataset for testing as in the **KITTI Split**.

Additionally, the data splits in nuScenes are based on scenes, making the tasks on nuScenes more challenging compared to KITTI. Further more, the **nuScenes Split 2** task includes fewer unknown categories and consequently fewer unknown instances, making it relatively simpler in terms of difficulty than the **nuScenes Split 1**.

B Implementation Details

Our 3D object discovery network (ODN3D) is designed an objectness branch, employed a binary classification branch and a standard box regression branch based on Object DGCNN [37] architecture with a voxel-based feature extractor from mmdetection3d [8]. The size of voxel is [0.1, 0.1, 0.2]. Same as the standard configuration, we use AdamW[19] optimizer and CBGS[45] for 20 epochs with a batch size of 4. The τ_1 , τ_2 corresponding to the Gaussian kernel functions ϕ_1 , ϕ_2 are set to 0.5, 0.05. In Stage 1, ODN3D is trained solely with instances of known classes. After this training phase, we use ODN3D to evaluate the training dataset. The query number for ODN3D is set to 300, meaning there are 300 3D object region proposals predicted for each frame. Since the ground truth of known instances is visible, we can directly perform GT filtering. We perform GT filtering frame by frame, removing 3D object region proposals that overlap with known class objects. Next, we sort the 3D object region proposals based on their objectness scores and select the top- k_o as 3D object region candidates, with top- k_o set to 30. Details on the hyperparameter analysis for top- k_o are provided in Section E.

BEVFormer[23] with ResNet-101[15] backbone is chosen as our camera baseline. We do not make any modifications to the model architecture of BEVFormer. In stage 1, we train BEVFormer for 18 epochs with a batch size of 1 solely with instances of known classes under the standard setting from mmdetection3d [8]. In Stage 2, unlike the standard BEVFormer setting, we change the input image queue length from 4 to 1. Additionally, the number of classes in the classification branch is set to $\mathcal{K} + 1$ (in Stage 1, the number of classes is \mathcal{K} , where \mathcal{K} represents the number of known object categories). Before training Stage 2, we reload the pretrained weights from the closed-set BEVFormer used in Stage 1, excluding the weights of the classification branch, and continue training for 6 epochs with a batch size of 1. The top- k_u is set to 10.

For the KITTI dataset, we maintained the same detection range parameters and evaluation standards as [6]. the detection range is $(0m, 70.4m)$ for the X axis, $(-40m, 40m)$ for the Y axis, and $(-3m, 1m)$ for the Z axis. The IoU threshold during evaluation is 0.7 for car and truck, 0.5 for pedestrian and cyclist, and 0.1 for the unknown objects, i.e., van and truck. The evaluation difficulty is moderate. For the nuScenes dataset, the detection range is $(-51.2m, 51.2m)$ for the X-axis, $(-51.2m, 51.2m)$ for the Y-axis, and $(-5m, 3m)$ for the Z-axis. During evaluation, the distance thresholds for both known and unknown categories are $(0.5m, 1m, 2m, 4m)$. All models are trained on $8 \times$ Tesla V100.

C Details on Joint Objectness Selection

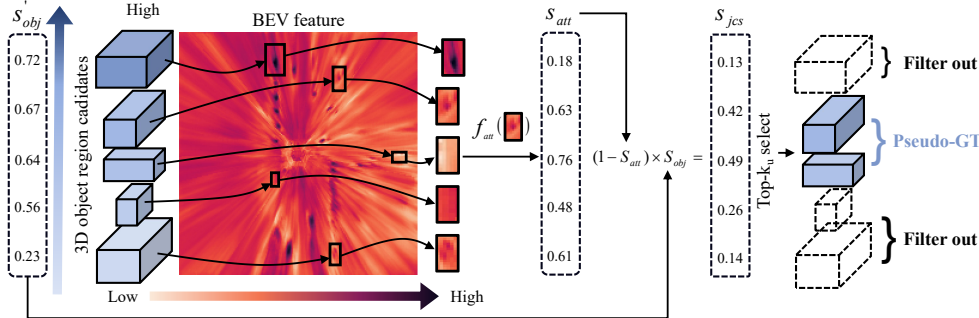


Figure 4: **Overview of JOS.** JOS computes corresponding attention score s_{att} for top- k_o candidates as the mean attention score within a BEV 2D region-of-interest. Then, we select the top- k_u candidates sorted by s'_{obj} as pseudo ground truth of unknown objects (pseudo-GT).

Here, we provide an example to demonstrate the JOS procedure, as shown in Fig. 4. Initially, we assume that k_o and k_u are set to 5 and 2, respectively. JOS takes 5 3D object region candidates as input and calculates the average attention score s_{att} over the BEV 2D regions of interest (with rotation) corresponding to these candidates.

In our setup, we aim to select candidates with high objectness scores and low attention scores as pseudo-labels for unknown objects. Therefore, we multiply the objectness scores of the 3D object region candidates by $1 - s_{att}$ obtained in the previous step to compute s_{jcs} . Finally, we sort the candidates based on s_{jcs} and select the top 2 as pseudo-labels for unknown objects.

D Details on OW-DETR Baselines

In this section, we provide implementation details for baselines. Compared to the method of generating pseudo-labels using features, we refer to the OW-DETR[14] approach to design two different feature extraction methods. To avoid confusion, we have named them DETR3D+OW-DETR, BEVFormer+OW-DETR, respectively, to distinguish between them, as shown in Fig. 5.

E Sensitivity Analysis k_o after Ground Truth Filtering

We vary k_o , Fig. 6 shows the analysis of k_o selected proposals sorted by s_{obj} . The top- k_o proposals after GT Filtering indicated the number of 3D region candidates which obtain a potential unknown

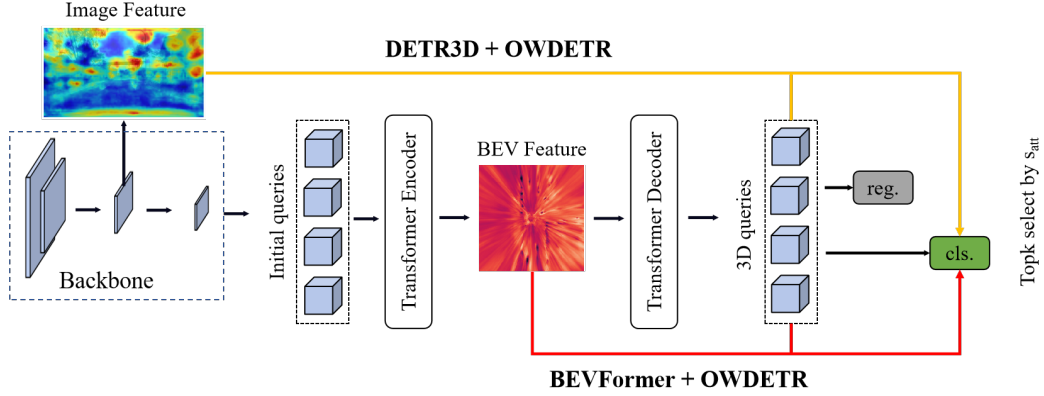


Figure 5: Different adaption of OW-DETR approach.

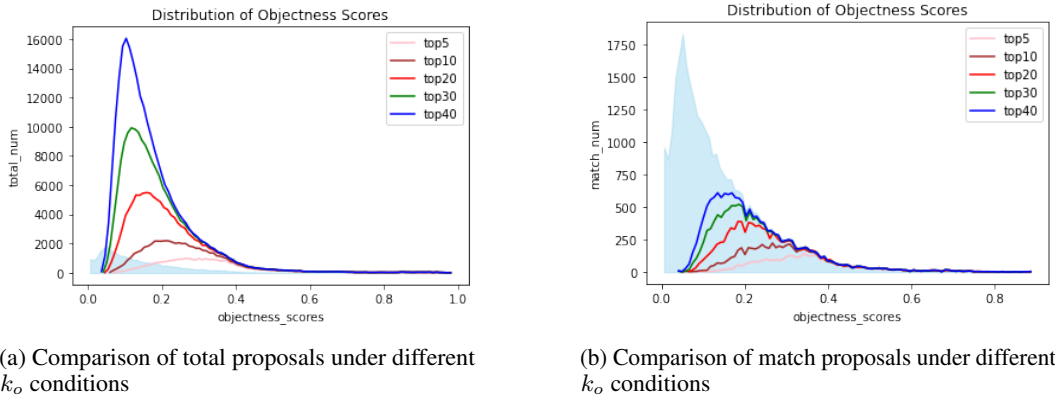


Figure 6: Analysis of k_o . The light blue shaded area represents the number of proposals from the ODN3D that match with instances of unknown ground truth, as well as the distribution of scores. In Fig. a and b, the sizes of the shaded areas are the same.

object. We extract the top- k_o proposals from each frame to serve as the 3D object region candidates fed into the JOS module. As observed in Fig. 6a, each curve indicates the number of 3D object region candidates across different score distributions, with the area under the curve representing the total number of extracted 3D region candidates. Subsequently, we match these candidates with the unknown ground truth to determine the corresponding number of matches. Correspondingly, in Fig. 6b, each curve displays the number of 3D object region candidates matching the ground truth across different score distributions. Thus, the area under each curve represents the total number of 3D object region candidates matching the ground truth. Since the selection of k_o is related to the unknown ground truth, we did not choose a value with a high proportion, as shown in Tab. 8. Instead, we selected a lower value to demonstrate the effectiveness of our method.

Table 8: The proportion of matched candidates among total candidates.

top- k_o	5	10	20	30	40
match/total(%)	12.4	10.4	8.2	7.0	6.1